5-9-2015

Bond Patterns in the Ground States of Quasi-One Dimensional 1/4-Filled Organic Superconductors

Andrew Bryan Ward

Follow this and additional works at: https://scholarsjunction.msstate.edu/td

Bond patterns in the ground states of quasi-one dimensional

1/4-filled organic superconductors

By

Andrew Bryan Ward

A Thesis
Submitted to the Faculty of
Mississippi State University
in Partial Fulfillment of the Requirements
for the Degree of Master of Science
in Physics
in the Department of Physics and Astronomy

Mississippi State, Mississippi

May 2015

Bond patterns in the ground states of quasi-one dimensional

1/4-filled organic superconductors

By

Andrew Bryan Ward

Approved:

_____

R. Torsten Clay
(Major Professor)

_____

Seong-Gon Kim
(Committee Member)

_____

Mark A. Novotny
(Committee Member)

_____

Henk F. Arnoldus
(Graduate Coordinator)

_____

R. Gregory Dunaway
Professor and Dean
College of Arts & Sciences

Name: Andrew Bryan Ward

Date of Degree: May 9, 2015

Institution: Mississippi State University

Major Field: Physics

Major Professor: Dr. R. Torsten Clay

Title of Study: Bond patterns in the ground states of quasi-one dimensional 1/4-filled organic superconductors

Pages of Study: 40

Candidate for Degree of Master of Science

Organic conductors are of considerable interest to the condensed matter community. In contrast to conventional metal conductors, these organic materials allow for large variability in their construction giving both quasi-one and two dimensional behavior. Organic superconductors also give useful insight into the properties of general superconductivity as well as insight into the properties of strongly correlated electronic materials. These materials exhibit interesting phenomena like spin-Peierls, antiferromagnetic, and superconducting phases. The aim of this thesis is not only to inform the reader of various studies into organic superconductors but also to advance research into these materials through massively parallel numerical methods. This thesis will cover two studies: a quantum Monte Carlo study on an infinite one-dimensional chain and an exact diagonalization study on a 16-site two-dimensional lattice. These studies will be used to better understand the charge and bond behavior of quasi-one dimensional 1/4-filled organic superconductors.

DEDICATION

To my parents.

ACKNOWLEDGEMENTS

TABLE OF CONTENTS

LIST OF TABLES

LIST OF ABBREVIATIONS

1D One Dimensional

2D Two Dimensional

CTS Charge Transfer Solid(s)

QMC Quantum Monte Carlo

SSE Stochastic Series Expansion

K kelvin

Pa Pascals

NMR Nuclear Magnetic Resonance

BCS Bardeen, Cooper, and Schrieffer

SP spin-Peierls

CO Charge Order

MI Metal-Insulator

AFM Antiferromagnetic

FCO Ferroelectric Charge Order

SC Superconductivity

DM dimer-Mott

CDW Charge Density Wave

BOW Bond Order Wave

BCDW Bond Charge Density Wave

$\mathbf{k}_F$ Fermi Wave Vector

SMWM Strong-Medium-Weak-Medium

SWSW' Strong-Weak-Strong-Weak'

TMTSF tetramethyl-tetraselenafulvalene

TMTTF tetramethyl-tetrathiafulvalene

EDO-TTF ethylene-dioxytetrathiafulvalene

MEM(TCNQ)$_2$ morpholinium-ditetracyanoquinodimethanide

PF$_6$ hexafluorophosphate

AsF$_6$ hexafluoroarsenate

SbF$_6$ hexafluoroantimonate

ClO$_4$ perchlorate

TaF$_6$ hexafluorotantalate

CHAPTER 1

INTRODUCTION

1.1 Outline of Thesis

The following chapters examine numerical studies of $\frac{1}{4}$-filled quasi-one dimensional organic superconductors. First, we will consider the various models and methods used as well as briefly survey the types of materials to be studied, specifically $\frac{1}{4}$-filled quasi-one dimensional CTS (charge transfer solids). We will then study the differing bond patterns in $\frac{1}{4}$-filled quasi-one dimensional CTS utilizing quantum Monte Carlo and finite size scaling techniques. Finally, we will study the magnetic ground states of these materials, specifically $(TMTTF)_2X$, via a self-consistent exact diagonalization method. By the end of this thesis, the reader should have a solid fundamental understanding of the bond and charge ordering of $\frac{1}{4}$-filled quasi-one dimensional organic superconductors as well as considerable knowledge of current numerical methods used in studying these materials.

CHAPTER 2

REVIEW OF MODELS AND METHODS

2.1 Survey of quasi-1D Organic Superconductors

John Bardeen, Leon Cooper, and John Robert Schrieffer proposed the first success-
ful microscopic theory of superconductivity in 1957, the well known BCS theory [1]. At
around the same time the search for highly conducting organic polymers began. In 1964,
W. A. Little [15] proposed the possibility of superconducting organic polymers with very
high transition temperatures. Little's superconducting polymers have yet to be synthesized,
but his work sparked scientific interest in finding organic superconductors. Since then,
there has been great interest in the synthesis of organic superconductors for decades culmi-
nating with the discovery of superconductivity in pressurized $(TMTSF)_2PF_6$ in 1980 [13].
A schematic of the molecular structure of TMTSF can be seen in Figure 2.1. A whole
family of superconductors was found in the $(TMTSF)_2X$ salts by changing the anion *X*,
where X = PF_6, AsF_6, SbF_6, ClO_4, TaF_6, etc. Another family of organic superconductors
can be found by replacing the selenium atoms with sulfur atoms, yielding the $(TMTTF)_2X$
salts. Note that the molecular structure of the TMTTF materials is the same as the TMTSF
materials (see Figure 2.1) except that the selenium atom in TMTSF is replaced with sulfur
in TMTTF. There are some open problems with studying these materials. Experimen-
tally, the $(TMTTF)_2X$ crystals are very small, too small for study with many methods such

2

as neutron diffraction. Some properties of various phenomena present in these organic superconductors, including some details of SP (spin-Peierls) and SC (superconducting) transitions, are not well known experimentally. Numerical modeling of these salts proves useful, but is also limited. Limitations on system size prevent the examination of 2D (two dimensional) lattices at infinite system size.
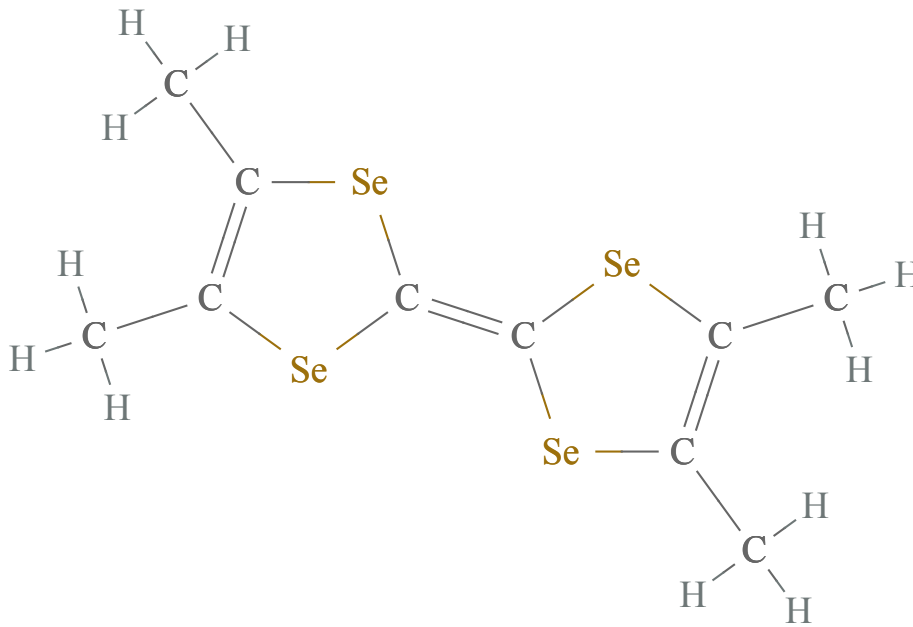
Figure 2.1

Molecular structure of the TMTSF salts

Se represents a selenium atom, C a carbon atom, and H a hydrogen atom.

2.2 Lanczos Exact Diagonalization and the Hubbard Model

Consider the following Hubbard Hamiltonian.

$$H = - \sum_{<ij>,\sigma} t_{ij}(c_{i,\sigma}^{\dagger}c_{j,\sigma} + H.c.) + U \sum_{i} n_{i,\uparrow}n_{i,\downarrow} + V \sum_{<ij>} n_i n_j \qquad (2.1)$$

In Eq. 2.1, t is the hopping energy, V is the intersite Coulomb interaction, U is the on-site Coulomb interaction, $c_{i,\sigma}^{\dagger}$ and $c_{j,\sigma}$ are the Fermion creation and annihilation operators respectively, $n_{i,\sigma} = c_{i,\sigma}^{\dagger}c_{i,\sigma}$ is the density operator, and $n_i = n_{i,\uparrow} + n_{i,\downarrow}$.

The zero-temperature ground state of this Hamiltonian can be calculated via Lanczos exact diagonalization. This method allows us to determine the lowest energy eigenvalue and its corresponding eigenstate without storing or diagonalizing the entire Hamiltonian matrix. The orthonormal basis for this model can be called the *occupation number basis* [14] and describes all possible states containing *N* electrons on *M* sites and each config-uration is of the form $|spin \uparrow occupancies\rangle|spin \downarrow occupancies\rangle$. For example, for an 8-site $\frac{1}{4}$-filled system containing 4 electrons (2 spin $\uparrow$ and 2 spin $\downarrow$), a typical configuration is $|10001000\rangle|01000100\rangle$ where in this case "1" represents an occupied site and "0" rep-resents an unoccupied site. A fairly obvious problem with this type of method is the large number of possible configurations. Let N_s be the number of states and it can be shown that

$$N_s = \prod_{\sigma} \frac{N!}{N_{\sigma}!(N - N_{\sigma})!} \qquad (2.2)$$

For the 8-site $\frac{1}{4}$-filled example above, $N_s = 784$. The Lanczos procedure constructs a tri-diagonal matrix that is much smaller than the full Hamiltonian, but has the same lowest eigenvalue (ground state).

2.3 Self-consistent Lanczos and the Peierls-extended Hubbard Model

Consider the following Peierls-extended Hubbard Hamiltonian.

$$H = -\sum_i (t - \alpha\Delta_i) B_{i,\sigma} + \frac{K_1}{2} \sum_i \Delta_i^2 + U \sum_i n_{i,\uparrow} n_{i,\downarrow}$$

$$+ V \sum_i n_i n_{i+1} + \beta \sum_i v_i n_i + \frac{K_2}{2} \sum_i v_i^2 \qquad (2.3)$$

In Eq. 2.3, $B_{i,\sigma} = \sum_\sigma (c_{i+1,\sigma}^\dagger c_{i,\sigma} + H.c.)$, α and β are the inter and intrasite e-ph (electron-phonon) couplings, respectively, and v_i and Δ_i are the lattice distortions with corresponding model spring constants K_1 and K_2. With the inclusion of e-ph interactions we now consider another aspect of the Lanczos method: self-consistency. Considering the Hamiltonian in Eq. 2.3, certain self-consistency equations can be derived:

$$\frac{\partial\langle H\rangle}{\partial\Delta_i} = 0 \text{ and } \frac{\partial\langle H\rangle}{\partial v_i} = 0 \qquad (2.4)$$

Solving these equations leads to the following self-consistency conditions.

$$\Delta_i = -\frac{\alpha}{K_1}\langle B_{i,\sigma}\rangle \text{ and } v_i = -\frac{\beta}{K_2}\langle n_i\rangle \qquad (2.5)$$

The system starts off in one of a number of states depending on the model parameters with an arbitrary or selected choice of v_i and Δ_i. It could start in a state of uniform charge distribution or in a randomly constructed state. A tolerance is set, and with the self-consistency conditions, the system is iterated until the tolerance is met. Typically in this calculation, the tolerance will be set in the 7th or 8th decimal places. What this method allows us to do is scan the phase space, detecting changes in the bond and charge ordering along the way. The phase space used here is (t_b, V), where V is the intersite Coulomb repulsion and t_b is the hopping parameter in the b (or vertical, see Figure 4.1) direction. This thesis will show that using this method we can map out the ground state phase diagram

5

of (TMTTF)$_2$X for an 8×2 lattice in an effort to learn more about the zero-temperature SP phase.

2.4 Survey of Quantum Monte Carlo/Stochastic Series Expansion

Consider the Hamiltonian in Eq. 3.1 (to be discussed further in Chapter 3). The purpose of this method is to perform calculations on lattice sizes much larger than those reachable by Lanczos. Lanczos can perform calculations on lattice sizes up to about 20, where SSE (stochastic series expansion) can perform calculations on lattice sizes in the 100's in 1D (one dimension). To measure certain observables like the bond susceptibility, χ_B, or the charge susceptibility, χ_ρ, we must evaluate the partition function,

$$Z = Tr\{e^{-\beta H}\}. \tag{2.6}$$

In Eq. 2.6, β is the inverse temperature and H is the Hamiltonian. There are a number of methods used to evaluate Z. So called *world line methods* [8] evaluate path integrals in imaginary time and rely on the Suzuki-Trotter decomposition of $e^{-\beta H}$ [23, 24]. Another method was developed by *Handscomb* [7] using the power series expansion of $e^{-\beta H}$ to solve the Heisenberg ferromagnet. Decades later a more general approach utilizing the power series expansion of $e^{-\beta H}$ was introduced by *Sandvik* [21] called the Stochastic Series Expansion. In SSE the partition function is written as follows,

$$Z = \sum_\alpha \sum_{n=0}^{\infty} \frac{(-\beta)^n}{n!} \langle \alpha | H^n | \alpha \rangle. \tag{2.7}$$

The trace has been written as a sum over all diagonal elements of H in a conveniently chosen basis $|\alpha\rangle$. The power of the SSE method comes from the fact that, unlike world

line methods, we are able to sample from Eq. 2.7 without needing to discretize imaginary time. Further advancements to the SSE approach use directed-loop updates [25] that allow for better configuration sampling. Another convenient part of this method is the fact that the power series expansion of H can be accurately truncated. It can be shown [25] that the power series expansion can be truncated at an integer M, where M is directly proportional to the inverse temperature and the system size, $M \sim \beta N$. The method works by taking in an initial configuration (β, system size, filling, etc.) and randomly samples possible configurations that fit this input. Two loop updates are used to improve the sampling: diagonal update and operator loop update. The diagonal update changes the order of the operators in the configuration by inserting a null operator. The operator loop update acts to modify the configuration by changing the spin of electrons as well as creating and annihilating electrons. Once the updates are finished, each configuration is used to calculate certain observables and the average of all of these calculations is reported.

This method is very useful in studying purely one-dimensional strongly correlated systems. In 1D, there is no exponential loss of precision known as the "fermion sign problem". This is because in Eq. 2.7, all matrix elements have the same sign in the case of a 1D lattice. Unlike the exact diagonalization method described in Section 2.3, this method does not rely on the diagonalization of very large matrices and can therefore be used for large system sizes. Large system sizes allow for 1D calculations to be done at the limit of infinite system size with the use of finite size scaling. This thesis will show the use of this method in observing differing bond patterns in the ground states of $\frac{1}{4}$-filled quasi-1D organic su-

7

perconductors. These differing bond patterns will be observed in the (U, V) phase diagram of these materials.

CHAPTER 3

STUDY OF BOND PATTERNS IN ONE DIMENSIONAL $\frac{1}{4}$-FILLED CHARGE

TRANSFER SOLIDS

Among the $\frac{1}{4}$-filled quasi-one dimensional molecular charge transfer solids there ex-
ist two distinct classes of spin-Peierls transitions. This phase is characterized by both
charge and bond distortions giving it the name bond charge density wave (BCDW). The
two classes (BCDW1 and BCDW2) are distinguished by differing bond patterns along the
chain direction: either the pattern Strong-Medium-Weak-Medium or the pattern Strong-
Weak-Strong-Weak', where the Weak bond is stronger than the Weak' (Weak prime) bond.
Experimentally the SP transition temperature of CTS of the first type, SMWM, is much
higher than those of the second type SWSW'. This indicates that the small change in bond
patterns within the SP phase greatly affects the electronic behavior of the CTS. We show
that this behavior can be observed within the Peierls-extended Hubbard Model and calcu-
late the phase boundary in the infinite chain limit.

3.1 Differing Bond Patterns in $\cdots 1100 \cdots$ SP Region

In general, one expects two types of phase transitions with the $\cdots 1100 \cdots$ SP region:
a charge or bond transition at high temperature and a magnetic transition at low temper-
ature [5]. A well-known, well-studied example of this are the $(TMTTF)_2X$ organic salts

[2, 6, 16, 17, 18, 22]. These organic superconductors exhibit CO (charge order) and MI (metal-insulator) transitions at high temperature and SP, AFM (antiferromagnetism), and superconducting phases at low temperature, see the T-P (temperature-pressure) phase diagram in Figure 3.1. Another example is the MEM(TCNQ)$_2$ salt [9, 28]. Measurement of the spin susceptibility (see Fig. 6 in [9]) for this material shows a spin-Peierls transition at low temperature, around 18 K and a lattice dimerization at high temperature, around 335 K [9]. Not all $\frac{1}{4}$-filled 1D SP materials follow this pattern, however. (EDO-TTF)$_2$X for example has a single SP transition coincident with the MI transition at high temperature, around 280 K with X=PF$_6$ [19]. Another organic crystal, (BDTFP)$_2$X, also has a single metal-insulator transition at high temperature, around 175 K with X=(PF$_6$)(PhCl)$_{0.5}$ [10]. As shown below, these materials can be separated into two types: BCDW1 (SMWM) and BCDW2 (SWSW').

3.1.1 Difference between BCDW1 and BCDW2 Materials

Type 1 (BCDW1) materials exhibit the bond pattern SMWM and go through a single high temperature SP transition. Type 2 (BCDW2) materials exhibit the bond pattern SWSW' and go through both a low and high temperature transition. Both have the CO pattern $\cdots 1100 \cdots$, where "1" represents a charge rich site (0.5 + δ) and "0" represents a charge poor site (0.5 - δ). CO is a phase transition in which translational symmetry is broken and a system goes from a state of uniform charge density to non-uniform charge ordering. To understand this behavior one can examine the bond and spin behavior in Figure 3.2. The strongest bond in the SMWM pattern occurs in between two charge rich

10
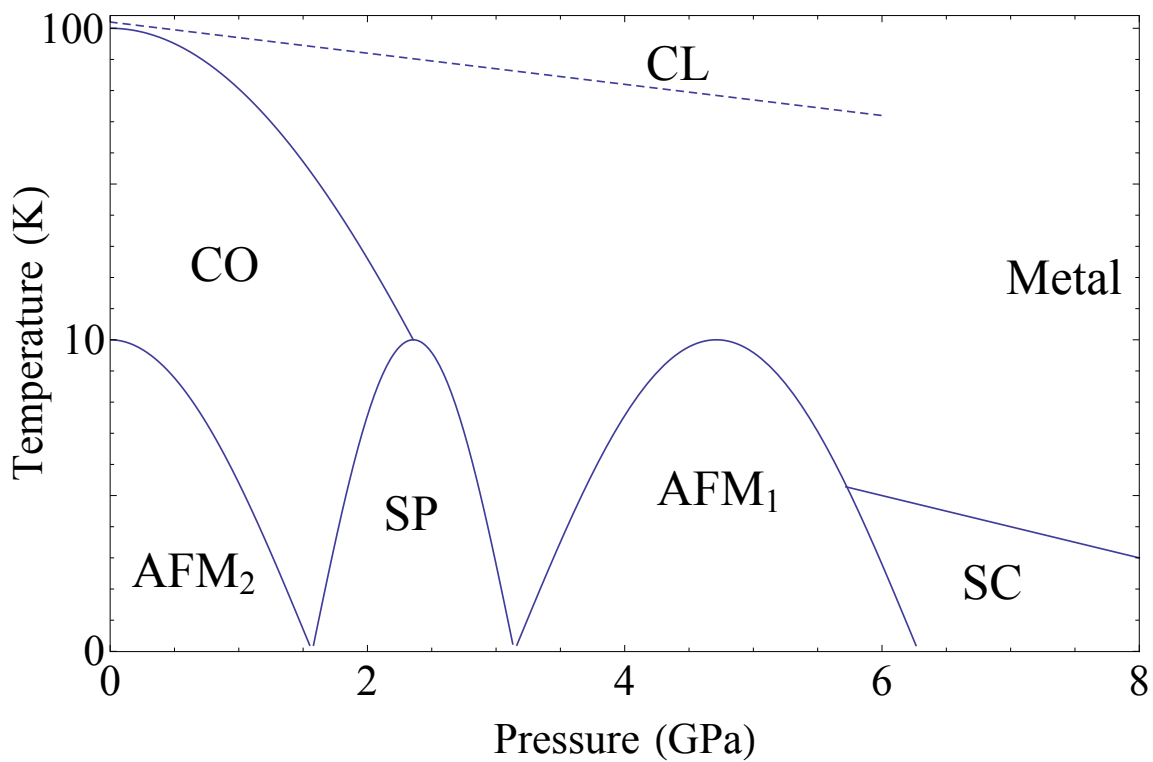
Figure 3.1

A generic Temperature vs Pressure phase diagram for (TMTTF)$_2$X

Here the phases shown are CO (charge order), SP (spin-Peierls), AFM (anti-ferromagnetism), CL (charge localization), and SC (superconducting). Made after Fig. 5 of [31]
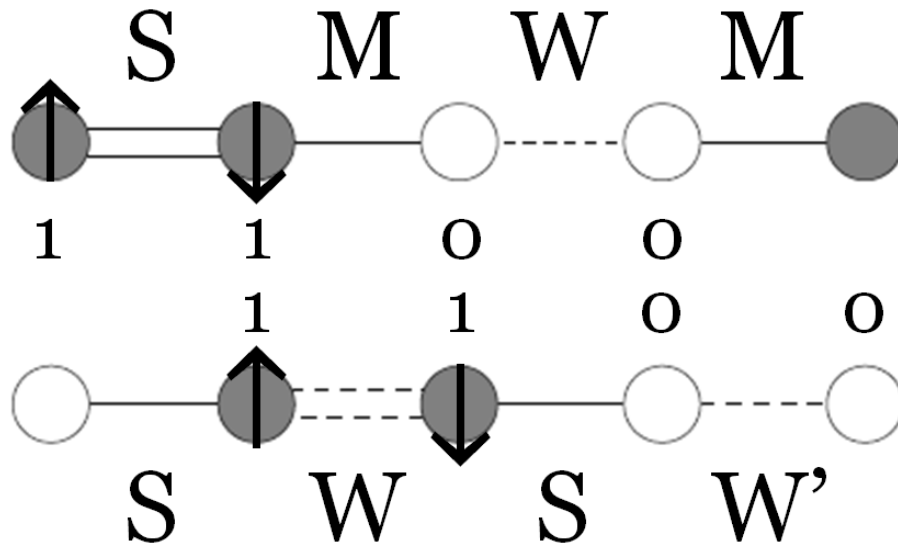
Figure 3.2

Bond and charge structure for BCDW1 (top) and BCDW2 (bottom) phases

"1" and a shaded circle represent a charge rich region, "0" and an empty circle represent a charge poor region. An up arrow represents a spin-up electron, a down arrow represents a spin-down electron. A solid line represents a stronger bond than a dashed line and double solid lines represent a stronger bond than a single solid line.

regions, 1=1. A spin singlet forms between the two "1" sites. The two "1" sites can be seen as a single charge rich site and the two charge poor sites can be seen as a single charge poor site, resulting in an effective $\frac{1}{2}$-filled lattice of charge order $\cdots 2020 \cdots$. In this effective $\frac{1}{2}$-filled lattice, only a single phase transition is expected: a transition from uniform charge density and uniform bond order, $\cdots 1111 \cdots$ to $\cdots 2020 \cdots$. Because the singlet coincides with the strongest bond, the spin gap is large with a high T_{sp}. This generalization cannot be made for the SWSW' lattice as a singlet does not coincide with the strongest bond, allowing for both low and high temperature transitions. The high temperature transition is either a lattice dimerization, as with MEM(TCNQ)$_2$, or a $\cdots 1010 \cdots$ CO, as with (TMTTF)$_2$X.

3.1.2 Peierls-extended Hubbard Model Hamiltonian

The model I consider is given by the following Hamiltonian.

$$H = -\sum_{i,\sigma}[t - \alpha\Delta_i]B_{i,\sigma} + \frac{K_1}{2}\sum_i \Delta_i^2 + U\sum_i n_{i,\uparrow}n_{i,\downarrow} + V\sum_i n_{i+1}n_i \tag{3.1}$$

Where $B_{i,\sigma} = \sum_\sigma(c^\dagger_{i+1,\sigma}c_{i,\sigma} + H.c.)$, t is the hopping energy, Δ_i is the deviation in the bond pattern from sites $i+1$ to i, V is the intersite Coulomb interaction, U is the onsite Coulomb interaction, α is the intersite electron-phonon coupling with the corresponding model spring constant K_1, $c^\dagger_{i,\sigma}$ and $c_{i,\sigma}$ are the Fermion creation and annihilation operators respectively, $n_{i,\sigma} = c^\dagger_{i,\sigma}c_{i,\sigma}$ is the density operator, and $n_i = n_{i,\uparrow} + n_{i,\downarrow}$. For convenience, energies will be given in units of t.

3.1.3 Bond Pattern

In order to calculate the boundary between the BCDW1 and BCDW2 phases, one must understand the nature of the bond and charge patterns in the 1D $\frac{1}{4}$-filled CTS. The bond and charge ordering in the $\cdots 1010 \cdots$ phase are dominated by their period 2 ($4k_F$) parts and correspond to a $4k_F$ charge density wave (CDW). The bond and charge ordering in the $\cdots 1100 \cdots$ phase are dominated by a cooperation between both period 2 and period 4 ($2k_F$) parts corresponding to a cooperative $2k_F$ CDW and a $2k_F + 4k_F$ BOW. The displacement of the jth molecule from equilibrium is given by u_j. In general, at $\frac{1}{4}$-filling u_j has $2k_F$ and $4k_F$ components:

$$u_j = u_0 \left[a_2 \cos \left(2k_F j - \phi_2 \right) + a_4 \cos(4k_F j - \phi_4) \right] \tag{3.2}$$

In Eq. 3.2, u_0 is the overall amplitude of the bond distortion, a_2 and a_4 are the amplitudes of the $2k_F$ and $4k_F$ parts respectively, and phase angles $\phi_2 = \frac{\pi}{4}$, $\phi_4 = 0$ are appropriate for BCDW1 and BCDW2 [27]. The switch over from SWSW' to SMWM occurs when the hopping integrals $t_{0,1}$ and $t_{1,2}$ are equal, with $t_{a,b} = t - \alpha(u_b - u_a)$. This implies a relationship between a_2 and a_4. Now let us evaluate $t_{0,1} = t_{1,2}$:

$$t - \alpha(u_1 - u_0) = t - \alpha(u_2 - u_1). \tag{3.3}$$

Evaluating Eq. 3.3 gives the following condition:

$$-\sqrt{2}a_2 + 4a_4 = 0 \tag{3.4}$$

We further assume the normalization condition $a_2 + a_4 = 1$. We now have a set of linear equations allowing us to solve for a_2 and a_4:

14

$$a_4 = \frac{\sqrt{2}}{4 + \sqrt{2}} = 0.2612 \tag{3.5}$$

With this we are able to evaluate the ratio of a_4 and a_2 explicitly:

$$\frac{a_4}{a_2} = \frac{\sqrt{2}}{4} \tag{3.6}$$

Note that the value of a_4 is incorrect in Ref. [27]. Now we define the bond distortion

between sites $j + 1$ and j, Δ_j.

$$\Delta_j = u_{j+1} - u_j$$
$$= -\sqrt{2}u_0 \left[a_2 \sin\left(\frac{\pi}{2}j\right) + \sqrt{2}a_4 \cos(\pi j) \right] \tag{3.7}$$
$$= u_0' \left[a_2' \sin\left(\frac{\pi}{2}j\right) + a_4' \cos(\pi j) \right]$$

Simplifying Δ_j gives the ratio of the $4k_F$ part of Δ_j to the $2k_F$ part:

$$\frac{a_4'}{a_2'} = \frac{\sqrt{2}a_4}{a_2} = \frac{1}{2} \tag{3.8}$$

Finally, reorganizing Δ_j yields

$$\Delta_j = \Delta_0[a_2' \cos(2k_F j - \phi_2) + a_4' \cos(4k_F j - \phi_4)] \tag{3.9}$$

In Eq. 3.9, $\phi_2 = \frac{3\pi}{2}$ and $\phi_4 = \pi$ are found by comparing Δ_j to u_j.

3.1.4 Observables

In order to calculate the boundary between the BCDW1 and BCDW2 phases within

the Peierls-extended Hubbard Model using the SSE method, a linear response function is

used, specifically the bond order susceptibility, χ_B.

$$\chi_B(q) = \frac{1}{N} \sum_{j,l} \int_0^\beta e^{iq(j-l)} \langle \tilde{B}_j(\tau) \tilde{B}_l(0) \rangle d\tau \tag{3.10}$$

Where N is the system size, β is inverse temperature, $\tilde{B}_j(\tau) = e^{-\tau H}\tilde{B}_j e^{\tau H}$, $\tilde{B}_j = B_j - \langle B \rangle$. Consider also the charge susceptibility, χ_ρ

$$\chi_\rho(q) = \frac{1}{N}\sum_{j,l}\int_0^\beta e^{iq(j-l)}\langle \tilde{n}_j(\tau)\tilde{n}_l(0)\rangle d\tau \tag{3.11}$$

Where n_j is the charge density operator.

3.1.5 Use of Stochastic Series Expansion / Quantum Monte Carlo

Quantum Monte Carlo simulations are used to calculate the bond order susceptibility at the limit of 0+ electron-phonon coupling. The method used here is the Stochastic Series Expansion with directed loop updates [25]. This system is purely one dimensional, allowing us to calculate the bond order susceptibility, χ_B, free of the Fermion sign problem that limits Hubbard model studies at higher dimensions. Secondly, this method is absent of Trotter discretization of imaginary time and is therefore statistically exact in one dimension. This method also allows for the use of very large system sizes compared to self-consistent methods. Large system sizes favor the use of finite size scaling and allow us to ignore finite size effects. The inverse temperature, β, is chosen to be large such that the method gives ground state results. In this case, we choose $\beta = 512$.

3.1.6 Boundary Between BCDW1 and BCDW2 Phases

In Figure 3.3 the charge susceptibility, χ_ρ, is shown. Our QMC calculations do not provide a direct measurement of the charge order amplitude in the BCDW1/BCDW2 phases; however, the charge susceptibility can be calculated. The charge susceptibility gives useful insight into the behavior of the charge order. As seen in Figure 3.3, χ_ρ in the BCDW1

phase has a $2k_F$ peak as well as a very large $4k_F$ peak, where χ_ρ in the BCDW2 phase is dominated only by a $2k_F$ peak. This indicates that the $2k_F \cdots 1100 \cdots$ CO will be stronger in the BCDW1 phase, consistent with the higher T_{SP} found there. Plots of charge density and bond order versus site number were made from a $\frac{1}{4}$-filled 16-site Lanczos exact diagonalization calculation. Charge density and bond order plots for the BCDW1 and BCDW2 phases can be found in Figure 3.4 and Figure 3.5, respectively.

3.2   Discussion of Bond Order Susceptibility

The bond order susceptibility, χ_B, measures the effect of perturbations to the bond strength at different wave vectors. The change over from SMWM (BCDW1) to SWSW' (BCDW2) occurs when the $4k_F$ part becomes significant compared to the $2k_F$ part. This can be measured by taking the ratio of the $4k_F$ part of the bond order susceptibility with respect to the $2k_F$ part, $\chi_B(4k_F)/\chi_B(2k_F)$. By using Δ_j as the form of the bond distortion in Eq. 3.10, it can be shown that

$$\frac{\chi_B(4k_F)}{\chi_B(2k_F)} = \frac{4a_4^{2\prime}}{a_2^{2\prime}} \tag{3.12}$$

Recalling that $\frac{a_4'}{a_2'} = \frac{1}{2}$ gives

$$\frac{\chi_B(4k_F)}{\chi_B(2k_F)} = 1 \tag{3.13}$$

This tells us that the switch over from BCDW1 to BCDW2 occurs when the ratio of the $4k_F$ part of the bond susceptibility to the $2k_F$ part is greater than one, $\frac{\chi_B(4k_F)}{\chi_B(2k_F)} > 1$.
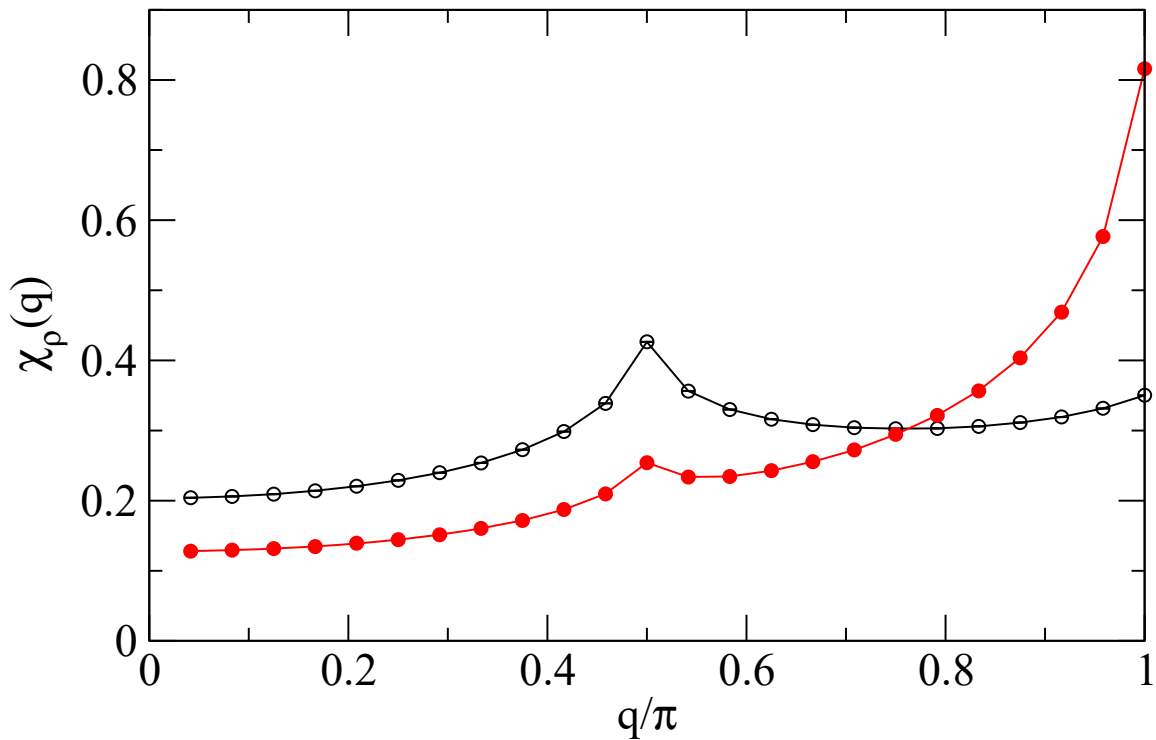
Figure 3.3

Charge susceptibility $\chi_B(q)$ as a function of q

Data taken from a 48 site chain for parameters in the BCDW1 and BCDW2 phases. Open symbols correspond to the BCDW1 region ($U = 3$, $V = 0.5$), and filled symbols to the BCDW2 region ($U = 6$, $V = 1$). Statistical errors are smaller than points. Note that $q = \frac{\pi}{2}$ is $2k_F$ and $q = \pi$ is $4k_F$.
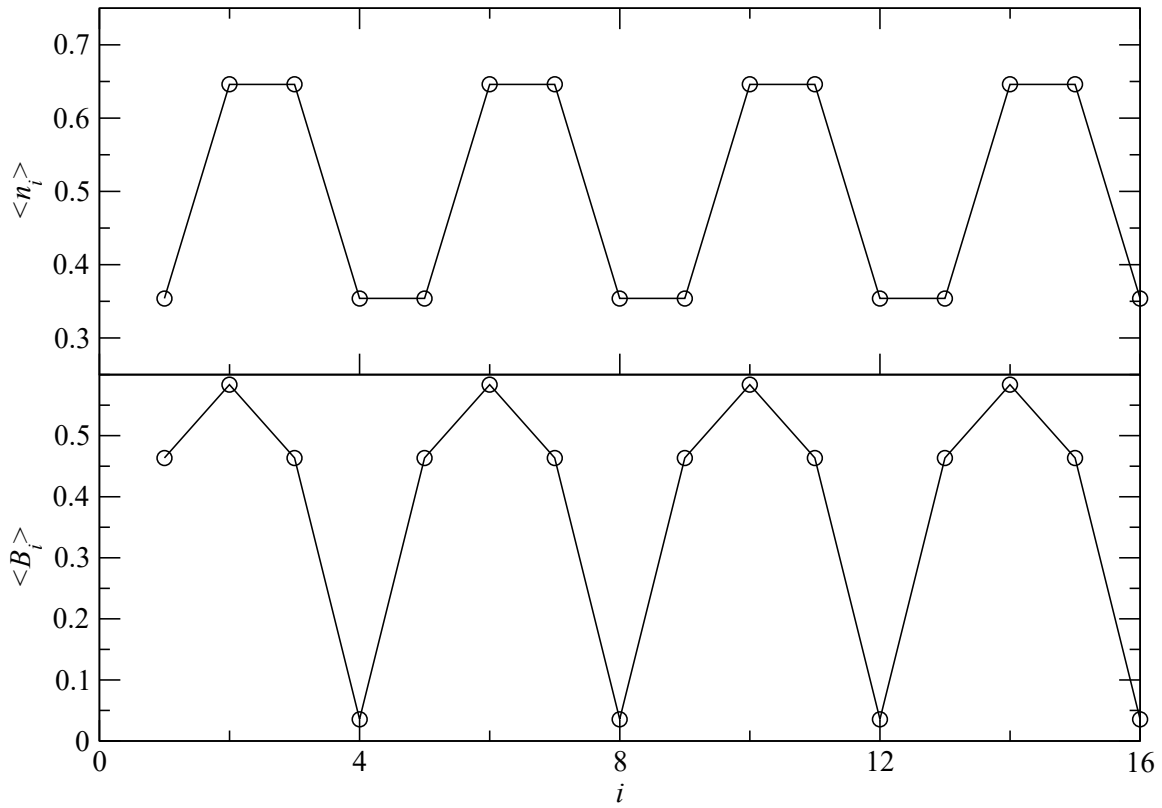
Figure 3.4

Charge density and bond order as a function of site number for the BCDW1 phase

$\langle n_i \rangle$ is the charge density, $\langle B_i \rangle$ is the bond order, and i is the site number.

Figure 3.5

Charge density and bond order as a function of site number for the BCDW2 phase

$\langle n_i \rangle$ is the charge density, $\langle B_i \rangle$ is the bond order, and i is the site number.

3.3 Use of Finite Size Scaling

It has been established above that the switch over from SMWM to SWSW' occurs when the ratio of the $4k_F$ part of the bond order susceptibility 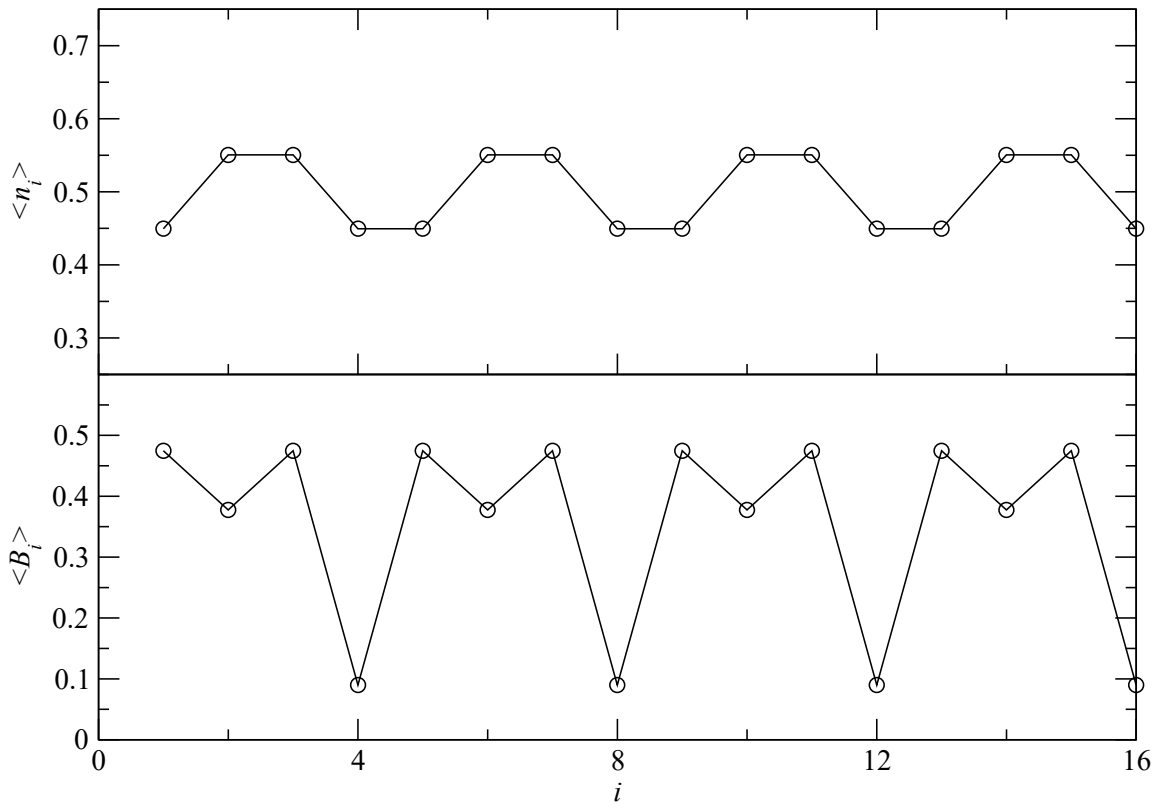with respect ot the $2k_F$ part, $\chi_B(4k_F)/\chi_B(2k_F)$, is equal to one. We intend to calculate this boundary in the (U, V) parameter space. In order to do this, $\chi_B(4k_F)/\chi_B(2k_F)$ is plotted versus the intersite Coulomb potential, V for a fixed value of the onsite Coulomb U and for a fixed system size, N, see Figure 3.6. As seen in Figure 3.6 this data fits to a straight line. Use of a linear regression yields the critical value of the Coulomb V, V_c, at which the ratio $\chi_B(4k_F)/\chi_B(2k_F) = 1$. Finite size scaling is done by plotting this V_c as a function of $1/N$. This can be seen in the inset of Figure 3.6. Again, this data fits to a straight line and a linear regression gives the y-intercept. The y-intercept represents the value of V_c in the limit $N \to \infty$, the infinite chain limit, for a particular Coulomb U. This procedure is repeated for various Coulomb U to map out the phase boundary in (U, V) space.

3.4 BCDW1/BCDW2 Boundary

The observed BCDW1/BCDW2 boundary can be seen in Figure 3.7. This boundary was determined in the physical region of the 1D $\frac{1}{4}$-filled CTS phase diagram. It is expected for actual materials that the Coulomb V will be less than half of the Coulomb U, $V < U/2$. For details of the $\cdots 1010 \cdots$ CO region, see [4]. It should also be noted that the slope of the BCDW1/BCDW2 curve gets flatter at increasing Coulomb U. This indicates that perhaps a minimum Coulomb V is required to realize the BCDW2 phase.
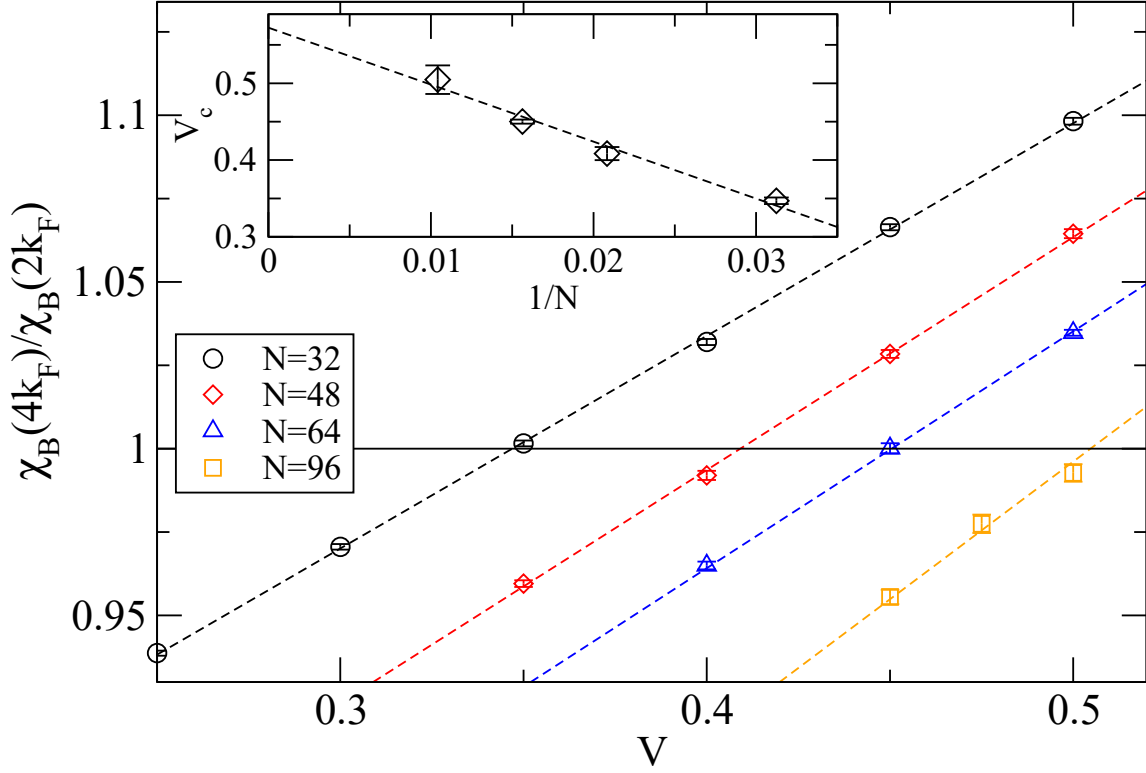
Figure 3.6

Ratio of $\chi_B(4k_F)/\chi_B(2k_F)$ as a function of V with $U = 6.25$

Circles, diamonds, triangles, and squares are for 32, 48, 64, and 96 site chains, respectively. The inset shows the finite-size scaling of the BCDW1/BCDW2 boundary determined from $\chi_B(4k_F)/\chi_B(2k_F) = 1$.
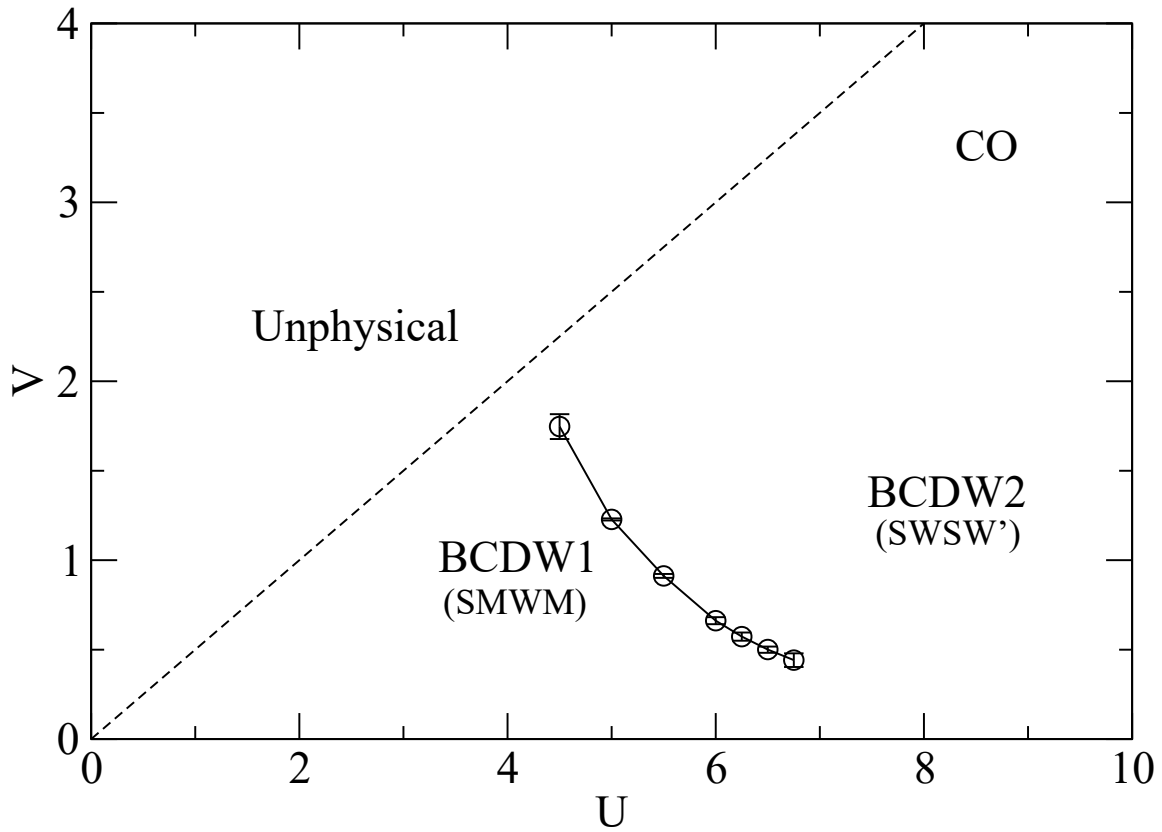
Figure 3.7

Zero temperature phase diagram of the $\frac{1}{4}$-filled 1D extended Hubbard model

Open points are the boundary between BCDW1 and BCDW2 regions. For the boundary to the CO region see Ref. [4]. The dashed line indicates the region of physical relevance for organic CTS, $V < \frac{U}{2}$.

3.5   Conclusion

As seen above, the BCDW1/BCDW2 phase boundary can be calculated within the Peierls-extended Hubbard Model in one dimension. This calculation was also done at the infinite chain limit, which to the best of our knowledge has not been done before. Attempts have been made to explain the single high SP transition temperature in $(EDO\text{-}TTF)_2X$ by considering exotic effects like molecular bending [26] and electronic polarization [11]. While these effects can be added to the Hubbard Hamiltonian, they are not necessary to observe the BCDW1/BCDW2 phase boundary. The BCDW1/BCDW2 phase boundary can be seen within the Peierls-extended Hubbard model considering only intersite and onsite Coulomb interactions.

CHAPTER 4

STUDY OF THE MAGNETIC GROUND STATES OF QUASI-ONE DIMENSIONAL

$\frac{1}{4}$-FILLED CHARGE TRANSFER SOLIDS

In this chapter, we examine a minimal model for the pressure dependent phases of the

(TMTTF)$_2$X salts, the extended Hubbard model on a two dimensional lattice with both

inter-site and on-site electron-phonon couplings. Recent calculations have suggested that

two distinct SP phases with different charge and bond ordering occur within this model. It

will be argued here that two distinct SP phases are not supported by experiment and are a

result of unsuitable parameter choices as well as finite-size effects within calculations. Pre-

sented here are the results of further numerical calculations as well as an investigation into

the effect of magnetic frustration on the AFM and SP phases. These results are published

in Ref. [29].

4.1 Experimental Signatures of Interchain Coupling

Among the quasi-one dimensional $\frac{1}{4}$-filled molecular charge transfer solids, an inter-

esting and well-studied example are the (TMTTF)$_2$X materials. As a function of pressure

the ground state of the (TMTTF)$_2$X salts is either one of two separate AFM phases, SP, or

superconducting, as seen in Figure 3.1. Increasing pressure is usually thought to decrease

the dimensionality of the crystal. The occurence of the SP phase (conventially believed to

be a one-dimensional effect) is then counterintuitive, as it enters at higher pressure than the first AFM phase. In this study, we seek to further examine the SP phase within the 2D Peierls- and Holstein- extended Hubbard model using Lanczos exact diagonalization on a 16-site $\frac{1}{4}$-filled lattice.

4.2   2D Peierls- and Holstein- extended Hubbard Model

The model I consider has the following Hamiltonian.

$$
\begin{aligned}
H = & -\sum_{<ij>_a,\sigma} t_{ij}(1 + u_{ij})(c_{i,\sigma}^{\dagger}c_{j,\sigma} + H.c.) - \sum_{<ij>_b,\sigma} t_{ij}(c_{i,\sigma}^{\dagger}c_{j,\sigma} + H.c.) \\
& + \frac{K_1}{2}\sum_{<ij>_a} u_{ij}^2 + U\sum_i n_{i,\uparrow}n_{i,\downarrow} + \sum_{<ij>} V_{ij}n_i n_j - \sum_i v_i n_i + \frac{K_2}{2}\sum_i v_i^2
\end{aligned}
\tag{4.1}
$$

In Eq. 4.1, t is the hopping energy, V is the intersite Coulomb interaction, U is the onsite Coulomb interaction, u_{ij} and v_i are bond and intramolecular distortions, respectively, with corresponding model spring constants K_1 and K_2, $c_{i,\sigma}^{\dagger}$ and $c_{j,\sigma}$ are the Fermion creation and annihilation operators respectively, $n_{i,\sigma} = c_{i,\sigma}^{\dagger}c_{i,\sigma}$ is the density operator, and $n_i = n_{i,\uparrow} + n_{i,\downarrow}$. Unlike the Hamiltonian in Eq. 3.1, this Hamiltonian absorbs the e-ph coupling, α, into the definition of K_1. What is important here is not the explicit value of α, but the value of the ratio $\frac{K_1}{\alpha}$ such that a decrease in $\frac{K_1}{\alpha}$ represents an increase in the strength of the inter-site e-ph coupling. Also, K_2 in the Hamiltonian now represents the ratio $\frac{K_2}{\beta}$, where β is the intra-site e-ph coupling.

4.2.1   Use of Lanczos Exact Diagonalization Method

A Lanczos exact diagonalization method with self-consistent solutions for u_{ij} and v_i was used to determine the lowest energy eigenvalue and its corresponding eigenstate for

a 16-site 2D lattice, see Figure 4.1. This eigenstate is used to determine certain correlation functions as well as bond and charge ordering. The charge density on the ith site is given by $\langle n_i \rangle$, the bond order is given by $\langle B_i \rangle$, the charge-charge correlation function is given by $\langle n_i n_j \rangle$, the spin-spin correlation function is given by $\langle (n_{i,\uparrow} - n_{i,\downarrow})(n_{j,\uparrow} - n_{j,\downarrow}) \rangle$. Here we wish to examine the P dependent behavior of the TMTTF salts by creating a zero temperature phase diagram in (t_b, V) space. We distinguish between the phases of these $\frac{1}{4}$-filled quasi-1D CTS by looking at differences in bond and charge patterns. Various phase transitions are expected in the quasi-1D picture of these organic salts, important ones among them are listed in Table 4.1, where "1" represents a charge rich site $(0.5 + \delta)$ and "0" represents a charge poor site $(0.5 - \delta)$. DM+SP is a dimerized Mott insulating phase created by a lattice dimerization (SP). DM+2DAFM is a coexisting dimerized Mott insulating phase and a two dimensional antiferromagnetic phase. FCO+2DAFM is a coexisting ferroelectric charge ordering phase with a 2D antiferromagnetic phase. For (TMTTF)$_2$X, the FCO phase is a 4k$_F$ $(\cdots 1010 \cdots)$ CO phase at high temperature. This phase is due to the intersite Coulomb interaction, V.

Table 4.1

Various phases of $\frac{1}{4}$ quasi-1D CTS

Phase	Charge	Description
DM+SP	$\cdots 1100 \cdots$	dimer-Mott + spin-Peierls
FCO+2DAFM	$\cdots 1010 \cdots$	Ferroelectric Charge Order + Antiferromagnetism
DM+2DAFM	uniform	dimer-Mott + Antiferromagnetism

4.3 Significance of Zero-Temperature Spin-Peierls Phase

Yoshimi *et al.* [30] have attempted to explain the pressure dependent behavior of Fabre salts which exhibit CO, AFM, and SP phases, see Figure 3.1. Experiments find two AFM phases [12, 31], AFM_1 at large P and AFM_2 at small P. Yoshimi *et al.* suggest that there also exist two distinct zero-temperature SP phases, SP_1 and SP_2. Here we point out that the occurence of two distinct SP phases contradicts experiments [12, 31] and is found by Yoshimi *et al.* because of unrealistic model parameters. Experiments [12, 31] emphasize cooperative interaction between the FCO and AFM_2 phases. In the experimental phase diagram [12, 31] T_{CO} and the Néel temperature in the AFM_2 phase both decrease with P (pressure). Thus charge occupancies in the FCO and AFM_2 phases are likely the same. In contrast, P increases [12, 31] the SP transition temperature, indicating that FCO and SP_2 phases compete. No CO was detected for $P > 0.5$ GPa in $(TMTTF)_2SbF_6$ [12, 31], in the P region where SP_2 phase occurs at lower temperature. It is then unlikely that SP_2 and FCO coexist at zero temperature.

4.4 Choice of Model Parameters

Before the Lanczos calculation can be done certain model parameters need to be set. The most important amongst them are the hopping parameters, t_{ij}, intersite Coulomb interactions, V, and the onsite Coulomb interactions, U. See Figure 4.1 for the structure of the lattice to be considered. a is the chain direction as well as the direction of the dimerization, b is the direction perependicular to the chain, and q is the diagonal. The hopping parameters in Ref [30] were calculated via first-principles density functional theory (DFT) for

(TMTTF)$_2$X in units of meV as $\{t_{a1}, t_{a2}, t_b, t_{q1}, t_{q2}\} = \{-155, -203, 26.2, -1.31, -3.29\}$ for X=PF$_6$ and $\{-149, -207, 16.4, -16.4, -9.73\}$ for X=SbF$_6$. The hopping parameters are generalized as follows: $t_{a1} = -0.8$, $t_{a2} = -1$, and $t_{q1} = t_{q2} = 0$ in units of t_{a2}, see Figure 4.1. The hopping parameters used by the authors in their model calculations are realistic. Their choice of Coulomb interactions is, however, unrealistic. The onsite Coulomb interaction assumed, $U/t_{a2} = 4$, is too small. In the purely electronic one dimensional model no 4k$_F$ ($\cdots 1010 \cdots$) CO occurs for this U [4, 22]. The assumed intersite Coulomb interactions, $V_b = 0$ and $V_q = V_a$, are also unrealistic. Given the lattice geometry, see Fig. 5 in [20], it is highly unlikely that $V_b \ll V_q$, and with large interchain separation $V_q = V_a$ is equally unrealistic. By observing the structure of (TMTTF)$_2$PF$_6$ it can be seen that the displacement of the stacks in the b direction is greater than in the a direction. We find that $4 \le U \le 8$ and $V_b \simeq V_q \ll V_a$ are more appropriate restrictions.

4.4.1   8 × 2 Lanczos Calculation

We repeated the 8×2 calculations in [30] with more realistic model parameters: $V_a = V$, $V_b = V_q = 0$ and $4 \le U \le 8$. We have three main observations. (i) For $V_a = V$, $V_b = V_q = 0$, we find a phase diagram similar to that in [30]. The (t_b, V) phase diagram by Yoshimi *et al.* can be seen in Fig. 3 of [30] and the (t_b, V) phase diagram from our work can be seen in Figure 4.5. The choice $V_q = V$, $V_b = 0$ is also not required to realize the FCO phase; FCO can be stabilized by antiferromagnetic superexchange along the t_b bonds. (ii) As U increases the FCO + SP phase narrows. (iii) For both these and the parameters assumed in [30], the width of the FCO + SP phase is directly proportional to
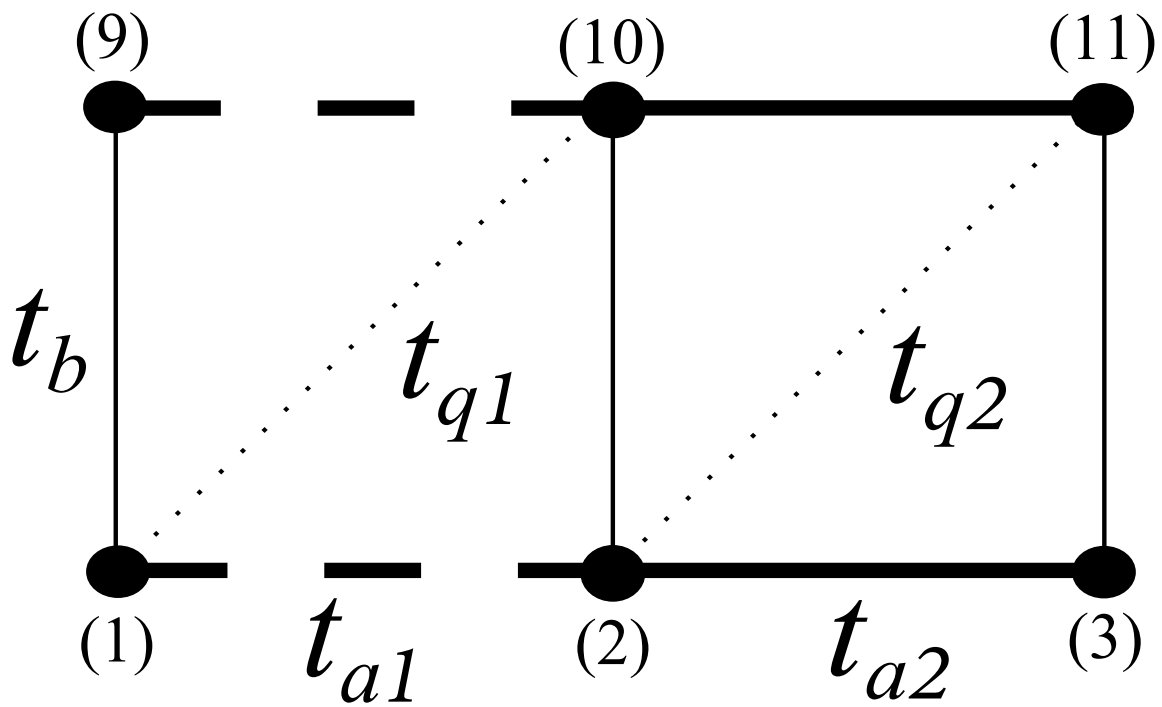
Figure 4.1

Lattice structure with corresponding hopping terms

For the 8×2 calculation, 16 total lattice sites were used. As seen from the site numbering, the figure continues to the right until the bottom chain reaches (8) and the top chain reaches (16). Consistent with the structure of $(TMTTF)_2X$ above the SP transition, the hopping parameters along the chain are dimerized.

the strength of the intersite electron phonon coupling (larger K_1 gives weaker coupling). Unconditional transitions in the thermodynamic limit occur in the limit of 0^+ phonon coupling. Importantly, point (iii) was not discussed in [30], and together with (ii) suggests that in the thermodynamic limit the FCO + 2DAFM and DM + SP phases may share a common border. Plots of charge density and bond order over the 16-site lattice in the DM+SP, DM+2DAFM, and FCO+2DAFM phases can be found in Figure 4.2, Figure 4.3, and Figure 4.4, respectively.

4.5 Conclusion

To understand the phase diagram one must consider thermodynamics. For large Coulomb interactions, the free energy is dominated by spin excitations. It was previously shown that the same DM + SP ground state can have two kinds of soliton spin excitations: (i) with local CO, or (ii) with uniform charge but local distortion [3]. In this picture, see Fig. 5 of [31], to the left of the line bisecting the SP phase, soliton excitations with local CO dominate at finite T; to the right occur excitations with uniform site charges. A unique SP ground state is expected at all pressures between AFM_1 and AFM_2.
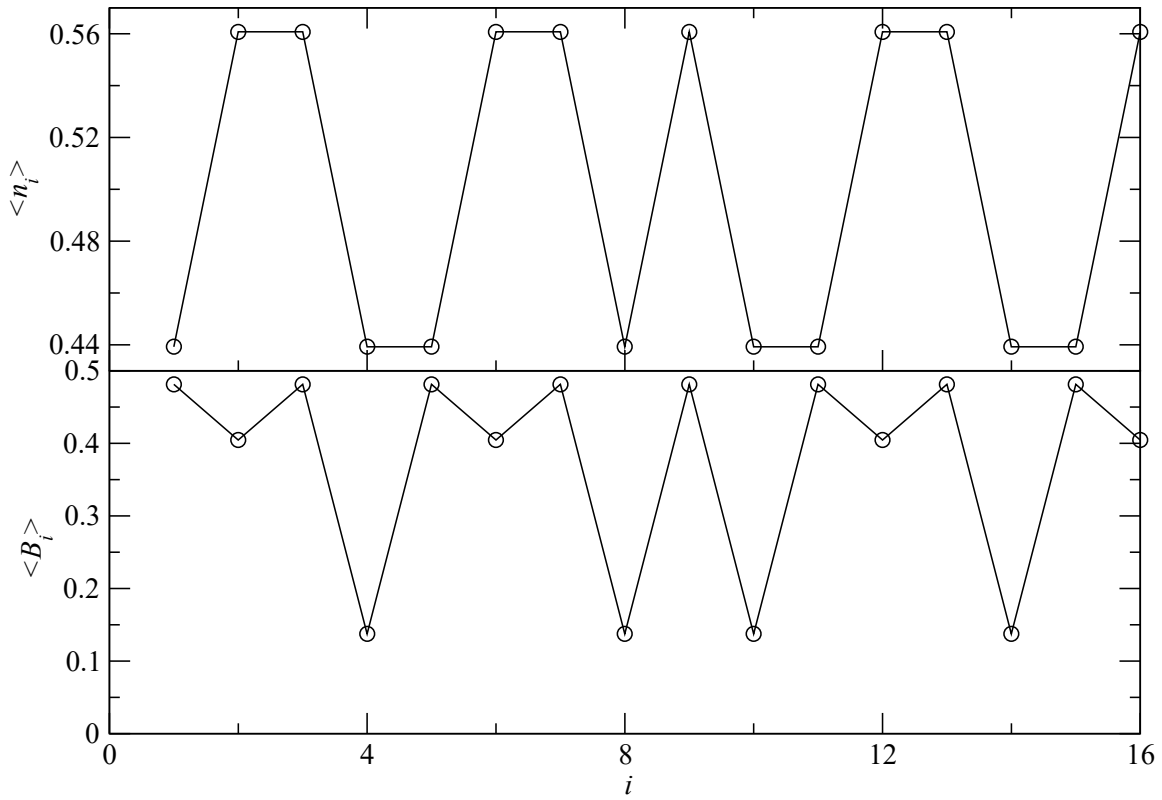
Figure 4.2

Charge density and bond order as a function of site number for the DM+SP phase

$\langle n_i \rangle$ is the charge density, $\langle B_i \rangle$ is the bond order, and i is the site number.

Figure 4.3

Charge density and bond order as a function of site number for the DM+2DAFM phase

$\langle n_i \rangle$ is the charge density, $\langle B_i \rangle$ is the bond order, and i is the site number.
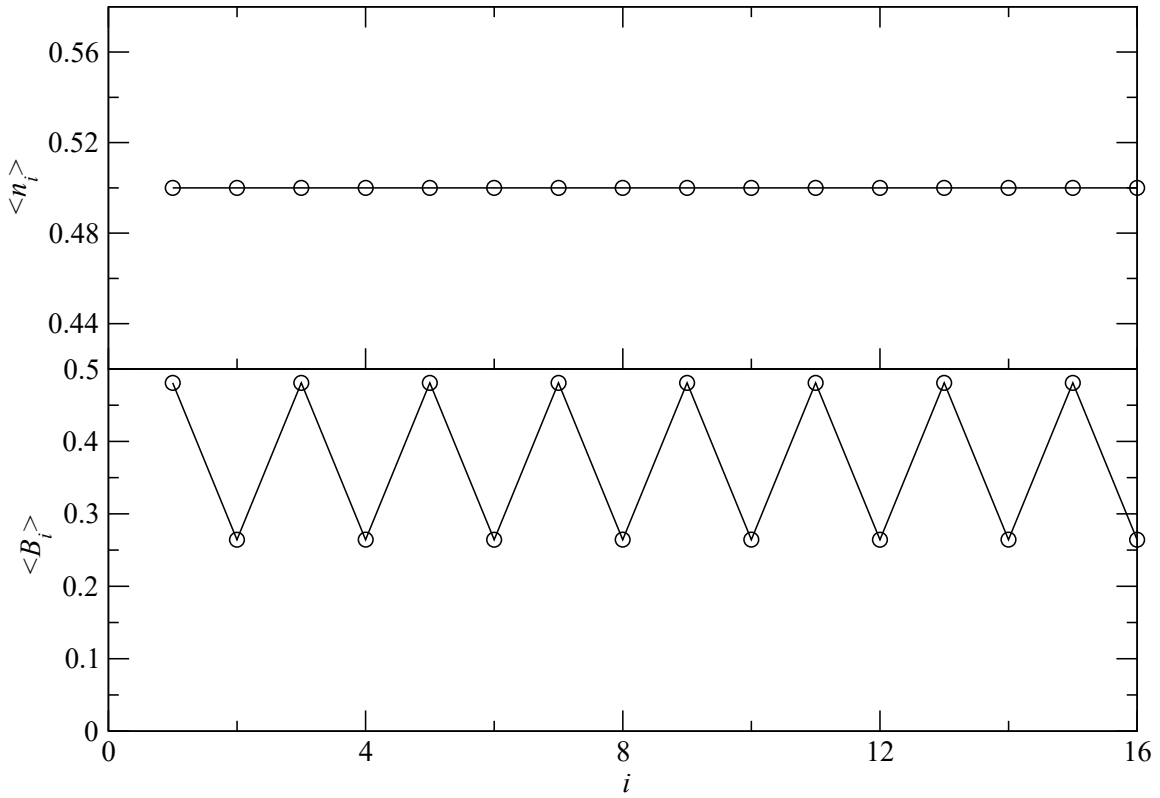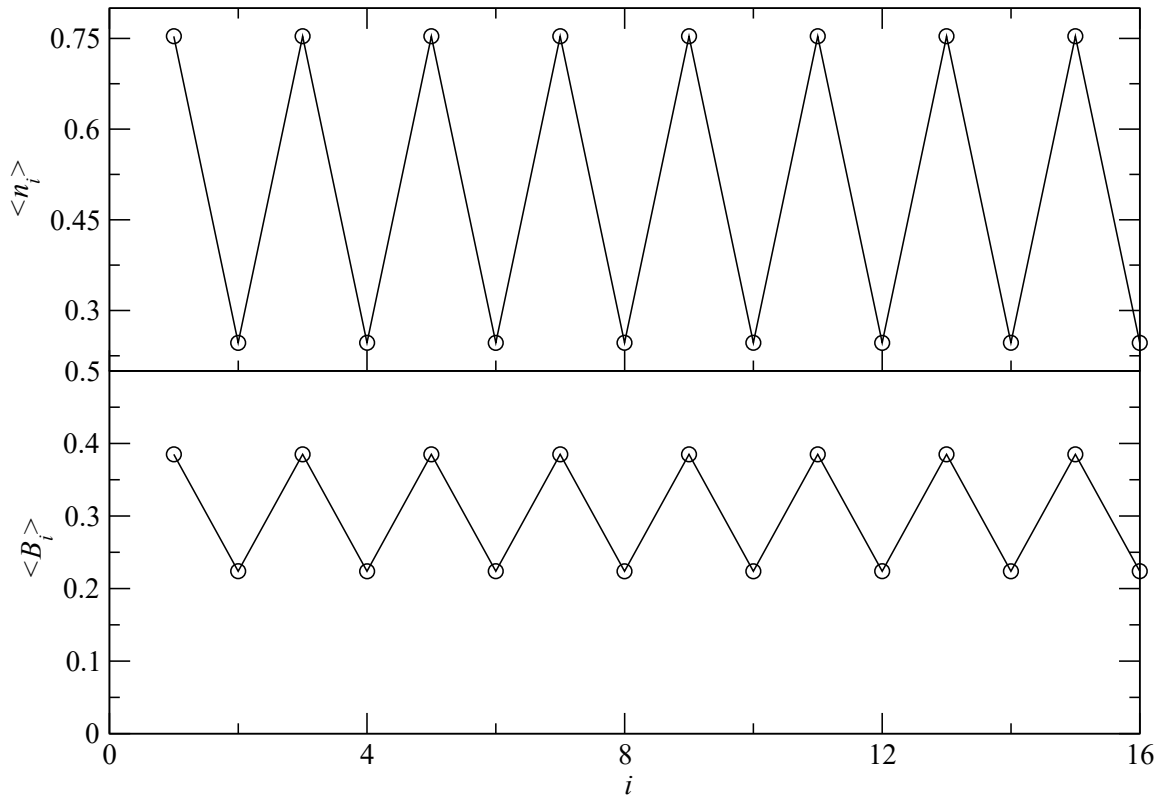
Figure 4.4

Charge density and bond order as a function of site number for the FCO+2DAFM phase

$\langle n_i \rangle$ is the charge density, $\langle B_i \rangle$ is the bond order, and i is the site number.
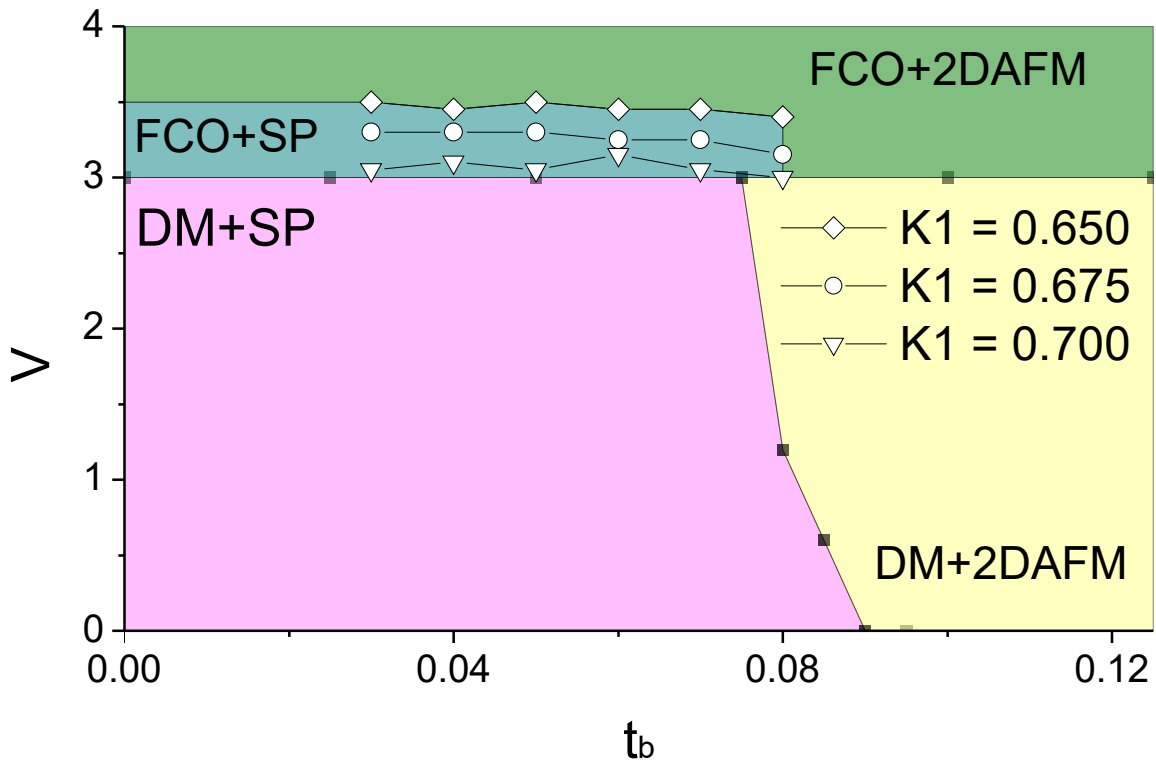
Figure 4.5

Phase diagram in (t_b, V) space for an 8×2 $\frac{1}{4}$-filled lattice

DM+SP represents a dimer-Mott insulating phase created by a lattice dimerization. FCO+SP is a proposed [30] phase of coexisting ferroelectric charge order and lattice dimerization. DM+2DAFM is a coexisting dimer-Mott insulator and two dimensional antiferromagnetic phase. FCO+2DAFM is a coexisting ferroelectric charge ordering phase with a two dimensional antiferromagnetic phase.

CHAPTER 5

CONCLUSIONS

This thesis has sought to introduce various concepts in studying bond patterns in $\frac{1}{4}$-filled quasi-1D organic superconductors as well as advance research interests in these materials. We have examined the differing bond patterns in these materials using QMC and finite size scaling. We have also studied the magnetic ground states in these quasi-1D materials via an 8×2 self-consistent Lanczos calculation.

5.1   Bond Patterns in quasi-1D $\frac{1}{4}$-filled CTS

We were able to observe the BCDW1/BCDW2 phase boundary within the 1D Peierls-extended Hubbard model. For the first time, this calculation has been done at the infinite chain limit. It has also been shown that this behavior is not unique to $(EDO\text{-}TTF)_2X$ and is shared by other quasi-1D $\frac{1}{4}$-filled CTS. It is an open question as to whether the BCDW2 phase requires $V > 0$.

5.2   Magnetic Ground States of quasi-1D $\frac{1}{4}$-filled CTS

By performing a self-consistent exact diagonalization calculation, we were able to better understand the SP transition in the quasi-1D $\frac{1}{4}$-filled $(TMTTF)_2X$ materials. It was found that the existence of a unique SP_2 transition is heavily dependent on the strength of

the e-ph coupling and most likely disappears at the thermodynamic limit. It is more likely that there exists a single unique SP phase in the ground state of $(TMTTF)_2X$. While useful, the exact diagonalization method used here is limited by small system size. Larger lattice calculations are needed for further study.

REFERENCES

[1] J. Bardeen, L. N. Cooper, and J. R. Schrieffer, "Theory of Superconductivity," *Phys. Rev. B*, vol. 108, 1957, p. 11751204.

[2] D. S. Chow, F. Zamborszky, B. Alavi, D. J. Tantillo, A. Baur, C. A. Merlic, and S. E. Brown, "Charge Ordering in the TMTTF Family of Molecular Conductors," *Phys. Rev. Lett.*, vol. 85, 2000, pp. 1698–1701.

[3] R. T. Clay, R. P. Hardikar, and S. Mazumdar, "Temperature-driven transition from the Wigner crystal to the bond-charge-density wave in the quasi-one-dimensional quarter-filled band," *Phys. Rev. B*, vol. 76, 2007, p. 205118.

[4] R. T. Clay, S. Mazumdar, and D. K. Campbell, "The pattern of charge ordering in quasi-one dimensional organic charge-transfer solids," *Phys. Rev. B*, vol. 67, 2003, p. 115121.

[5] R. T. Clay, J. P. Song, S. Dayal, and S. Mazumdar, "Ground state and finite temperature behavior of 1/4-filled band zigzag ladders," *J. Phys. Soc. Jpn.*, vol. 81, 2012, p. 074707.

[6] C. Coulon, G. Lalet, J. P. Pouget, P. Foury-Leylekian, A. Moradpour, and J. M. Fabre, "Anisotropic conductivity and charge ordering in $(TMTTF)_2X$ salts probed by ESR," *Phys. Rev. B*, vol. 76, 2007, p. 085126.

[7] D. C. Handscomb, "The Monte Carlo method in quantum statistical mechanics," *Proc. Cambridge Philos. Soc.*, vol. 58, 1962, p. 594.

[8] J. E. Hirsch, R. L. Sugar, D. J. Scalapino, and R. Blankenbecler, "Monte Carlo simulations of one-dimensional fermion systems," *Phys. Rev. B*, vol. 26, 1982, p. 5033.

[9] S. Huizinga, J. Kommandeur, G. A. Sawatzky, B. T. Thole, K. Kopinga, W. J. M. de Jonge, and J. Roos, "Spin-Peierls transition in N-methyl-N-ethyl-morpholinium-ditetracyanoquinodimethanide [MEM-$(TCNQ)_2$]," *Phys. Rev. B*, vol. 19, no. 9, May 1979, pp. 4723–4732.

[10] T. Ise, T. Mori, and K. Takahashi, "Preparation, crystal structures and electrical properties of PF_6 and AsF_6 salts of a novel furopyrazine-extended donor (BDTFP) with a two-leg ladder type orbital overlapping mode," *J. Mater. Chem.*, vol. 11, 2001, pp. 264–265.

[11] K. Iwano and Y. Shimoi, "Large electric-potential bias in an EDO-TTF tetramer as a major mechanism of charge ordering observed in its PF_6 salt: A density functional theory study," *Phys. Rev. B*, vol. 77, 2008, p. 075120.

[12] F. Iwase, K. Sugiura, K. Furukawa, and T. Nakamura, "C NMR study of the magnetic properties of the quasi-one-dimensional conductor $(TMTTF)_2SbF_6$," *Phys. Rev. B*, vol. 84, 2011, p. 115140.

[13] D. Jérome, A. Mazaud, M. Ribault, and K. Bechgaard, "Superconductivity in a synthetic organic conductor $(TMTSF)_2PF_6$," *J. Phys. (Paris) Lett.*, vol. 41, 1980, pp. L95–L98.

[14] H. Q. Lin and J. E. Gubernatis, "Exact diagonalization methods for quantum systems," *Computers in Physics*, vol. 7, 1993, p. 4.

[15] W. A. Little, "Possibility of synthesizing an organic superconductor," *Phys. Rev.*, vol. 134, 1964, pp. A1416–1424.

[16] S. Mazumdar, S. Ramasesha, R. T. Clay, and D. K. Campbell, "Theory of Coexisting Charge- and Spin-Density Waves in $(TMTTF)_2Br$, $(TMTSF)_2PF_6$, and α-(BEDT-$TTF)_2MHg(SCN)_4$," *Phys. Rev. Lett.*, vol. 82, 1999, pp. 1522–1525.

[17] P. Monceau, F. Nad, J. M. Fabre, and T. Nakamura, "Charge and anion ordering in $(TMTTF)_2X$ quasi-one-dimensional conductors," *J. Low T. Phys.*, vol. 142, 2006, p. 367.

[18] T. Nakamura, "Possible Charge Ordering Patterns of the Paramagnetic Insulating States in $(TMTTF)_2X$," *J. Phys. Soc. Jpn.*, vol. 72, 2003, pp. 213–216.

[19] A. Ota, H. Yamochi, and G. Saito, "A novel metal-insulator phase transition observed in $(EDO-TTF)_2PF_6$," *J. Mater. Chem.*, vol. 12, 2002, p. 2600.

[20] S. Ravy, "Diffuse X-ray scattering studies of molecular conductors," *Annu. Rep. Prog. Chem., Sect. C: Phys. Chem.*, vol. 103, 2007, pp. 223–260.

[21] A. W. Sandvik, "A generalization of Handscomb's quantum Monte Carlo scheme-application to the 1D Hubbard model," *J. Phys. A*, vol. 25, 1992, pp. 3667–3682.

[22] H. Seo, J. Merino, H. Yoshioka, and M. Ogata, "Theoretical aspects of charge ordering in molecular conductors," *J. Phys. Soc. Jpn.*, vol. 75, 2006, p. 051009.

[23] M. Suzuki, "Relationship between *d*-dimensional quantal spin systems and (*d+1*)-dimensional Ising Systems: Equivalence, critical experiments and systematic approximants of the partition function and spin correlations," *Prog. Theor. Phys.*, vol. 56, 1976, p. 1454.

[24] M. Suzuki, S. Miyashita, and A. Kuroda, "Monte Carlo simulation of quantum spin systems. I," *Prog. Theor. Phys.*, vol. 58, 1977, p. 1377.

[25] O. F. Syljuasen and A. W. Sandvik, "Quantum Monte Carlo with directed loops," *Phys. Rev. E*, vol. 66, 2002, p. 046701.

[26] M. Tsuchiizu and Y. Suzumura, "Peierls ground state and excitations in the electron-lattice correlated system (EDO-TTF)$_2$X," *Phys. Rev. B*, vol. 77, 2008, p. 195128.

[27] K. C. Ung, S. Mazumdar, and D. Toussaint, "Metal-Insulator and Insulator-Insulator Transitions in the Quarter-Filled Band Organic Conductors," *Phys. Rev. Lett.*, vol. 73, 1994, pp. 2603–2606.

[28] R. J. J. Visser, S. Oostra, C. Vettier, and J. Voiron, "Determination of the spin–Peierls distortion in N-methyl-N-ethyl-morpholinium ditetracyanoquinodimethanide [MEM(TCNQ)$_2$]: Neutron diffraction study at 6 K," *Phys. Rev. B*, vol. 28, 1983, pp. 2074–2077.

[29] A. B. Ward, R. T. Clay, and S. Mazumdar, "Comment on "Tuning the Magnetic Dimensionality by Charge Ordering in the Molecular TMTTF Salts," *Phys. Rev. Lett.*, vol. 108, 2014, p. 029701.

[30] K. Yoshimi, H. Seo, S. Ishibashi, and S. E. Brown, "Tuning the Magnetic Dimensionality by Charge Ordering in the Molecular TMTTF Salts," *Phys. Rev. Lett.*, vol. 108, 2012, p. 096402.

[31] W. Yu, F. Zhang, F. Zamborszky, B. Alavi, A. Baur, C. A. Merlic, and S. E. Brown, "Electron-lattice coupling and broken symmetries of the molecular salt (TMTTF)$_2$SbF$_6$," *Phys. Rev. B*, vol. 70, 2004, p. 121101.